Title

Current/Voltage Characteristics of the Short-Channel Double-Gate Transistor. Part I

Journal

SIAM Journal on Applied Mathematics, 78(2)

ISSN

0036-1399

Authors

Cumberbatch, Ellis

Smith, Stefan G Llewellyn

Publication Date

2018

DOI

10.1137/17m1121123

Peer reviewed

SIAM J. APPL. MATH.
Vol. 78, No. 2, pp. 877–896

CURRENT/VOLTAGE CHARACTERISTICS OF THE SHORT-CHANNEL DOUBLE-GATE TRANSISTOR. PART I*

ELLIS CUMBERBATCH† AND STEFAN G. LLEWELLYN SMITH‡

Abstract. The drift-diffusion equations relevant for application to current flow in the double gate transistor are addressed. In standard operation this device has both source and drain heavily doped with the silicon body at the intrinsic level. This situation means that there are two second-order elliptic partial differential equations containing an exponential nonlinearity representing the mobile electrons. For the ODEs governing electron flow source-to-drain away from narrow layers close to the gates, we obtain new exact and accurate approximate analytic solutions. Part II will include improvements close to the gates as boundary layers.

Key words. MOSFET, current-voltage relation, asymptotic analysis

AMS subject classifications. 68Q25, 68R10, 68U05

DOI. 10.1137/17M1121123

1. Introduction.

This is the first part of a two-part sequence investigating the solution of a set of nonlinear partial differential equations (PDEs) relevant to current flow in a transistor design of recent technological interest. This first part is being offered separately because of its *mathematical* interest: we have obtained an exact solution to the system of ordinary differential equations (ODEs) relevant to the solution behavior over part of the domain of interest for the full PDEs. Additionally these ODE solutions provide the outer solution when solutions in the complementary part of the domain are found and incorporated in a matched asymptotic (MAE) approach. This part of the work will be offered in Part II. In Part I, we also include an MAE solution for the ODE system as (a) it has an intriguing structure (7 layers) and (b) it provides insight into the overall solution behavior and consequently helps with analysis of the (complicated) exact solutions. Comparison of the analytic results with numerical solutions is provided for various approximations. Part II will provide solutions to the complete boundary value problem and will show comparisons with previous work (usually numerical) presented elsewhere.

The standard transistor used in the semiconductor industry is the MOSFET (metal-oxide-silicon field-effect transistor). The basic design incorporates a single gate. Current fabrication can place hundreds of millions of such transistors on a chip. For design purposes of chip performance (using SPICE software, say) the MOSFET is modeled as an assemblage of capacitances, resistances, and a diode, most of which have characteristics dependent on the applied voltages and on device parameters such as dimensions, material properties, and doping levels. These dependencies are modeled by the drift-diffusion equations (or by a quantum mechanical formulation for very small devices), which are nonlinear partial differential equations. Numerical solutions of these PDEs, though accurate, would be slow for design purposes of chips with many interconnected transistors, and approximate analytic solutions are used. When

*Received by the editors March 15, 2017; accepted for publication (in revised form) November 17, 2017; published electronically March 27, 2018.
http://www.siam.org/journals/siap/78-2/M112112.html

†Institute of Mathematical Sciences, Claremont Graduate University, Claremont, CA 91711 (ellis.cumberbatch@cgu.edu, https://www.cgu.edu/people/ellis-cumberbatch).

‡Department of Mechanical and Aerospace Engineering, Jacobs School of Engineering, UCSD, La Jolla, CA 92093 (sgls@ucsd.edu, http://web.eng.ucsd.edu/~sgls).

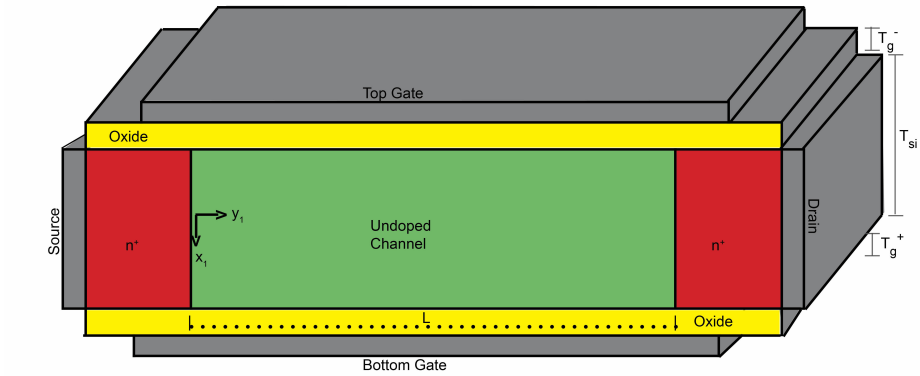

FIG. 1. *Double gate design.*

the channel length was large, the approximation for the transistor current/voltage behavior was obtained from a quasi-one-dimensional (quasi-1-D) solution, an ODE approximation. As channel lengths have been reduced, the ODE formulae have been amended empirically, as there are no PDE analytic solutions for relevant voltages.

There are two large complications for 2-D analytic solutions in the standard MOSFET case: (1) the geometry and (2) the presence of a free surface (the boundary between the active and passive regions in the silicon.) Ward [15] formulated an idealized free boundary problem for the drain/gate corner region, where the quasi 1-D solution is most affected by the 2-D geometry. He was able to obtain results that amended the quasi 1-D current/voltage formula for small drain voltages and large channel lengths.

Over the last decade the double-gate (DG) design, shown in Figure 1, has been fabricated and used successfully. (There are also cylindrical designs.) The DG is harder to fabricate, but its commercial use is increasing as it has desirable technological properties at the smaller channel lengths that are increasingly being utilized. The long channel ODE formulation for the DG device is available and is in use. There is a large bibliography of such work; see, for example [1, 11, 8].

The introduction of the DG transistor brings anticipation of progress toward analytic solutions of the drift-diffusion PDEs. The geometry is simpler: the silicon region is a rectangle. The doping in the silicon is weak (often it is at the intrinsic level) meaning that there is no free boundary. For the 2-D problem the case of threshold voltages allows a linearization, and techniques of separation of variables or conformal mapping have been applied [2, 6, 7].

To the authors' knowledge there have been no publications for the case of the short-channel DG transistor valid for voltages above the threshold when a linearization does not give accurate results. Numerical solutions (see Figure 2) indicate large electron densities along the channels bordering the two gates. Since these may be taken care of by the usual boundary-layer analysis it is necessary to solve the source-to-drain behavior.

Our work aims to provide a PDE solution for the DG device in a form suitable for SPICE application. In particular, in this paper, it provides an *exact* solution to the ODEs governing the drift-diffusion behavior from source to drain, valid down the central region of the device. This solution is complicated, but approximations are introduced that allow the current to be evaluated in terms of the voltage difference source-to-drain. In a subsequent paper the effect of a positive voltage applied at

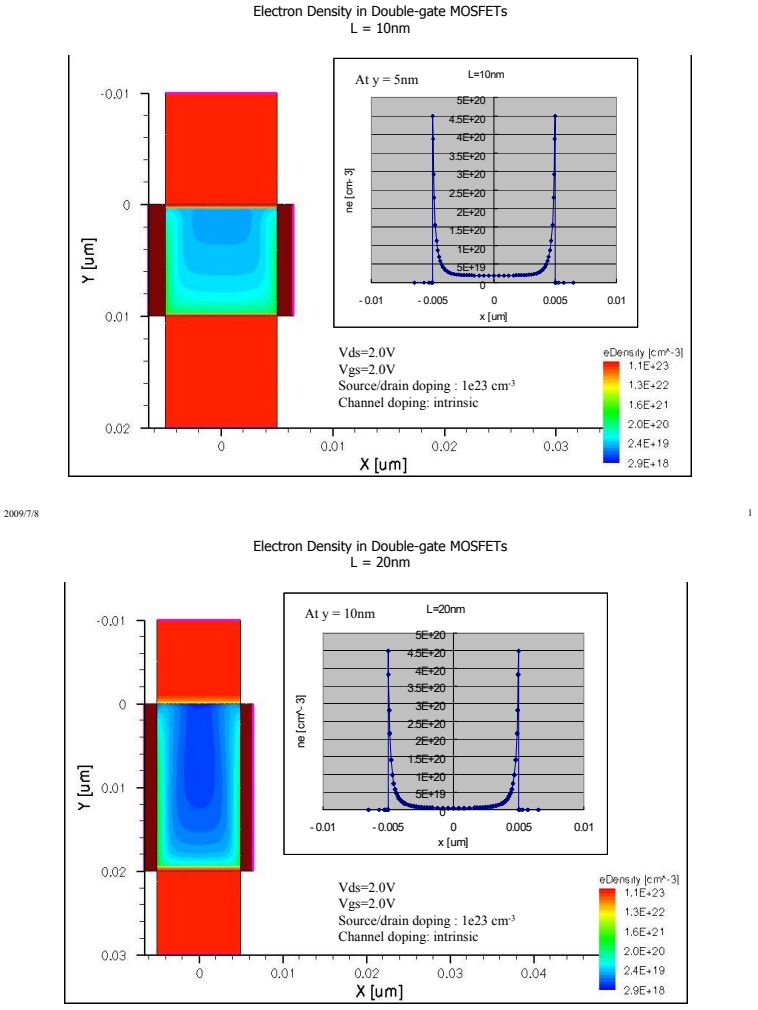

FIG. 2. *Typical DG electron densities* [14].

the gates that increases the electrons attracted to thin layers (channels) there (see Figure 2) will be included. The current in the central region is supplemented by contributions from these layers, and it is anticipated that this effect will be modeled by boundary-layer theory.

The full equations and boundary conditions are set out in the next section, together with a scaled version of these equations. Numerical solutions of the PDEs for short channel geometries show that there is a large central region of the device, away from narrow layers close to the gates, in which the solution is predominantly influenced by the voltage difference between source and drain. The solution in this central region is the focus of the present paper. The ODEs governing this region are addressed in section 3.

Standard transistors operate at low voltages (less than 2 volts). Even so, these voltages are large compared with the voltage relevant to electron displacement, the

thermal voltage. The inverse of this ratio is used as a small parameter in an MAE approach discussed in sections 4 and 5, where approximate solutions are obtained. Section 6 presents a complete exact analytic solution to the ODEs generated in section 3.

2. Governing equations and scaling. The physical set-up is shown in Figure 1. Only the case with symmetry about the center-line is treated: the gate (insulator) thicknesses are equal

$$T_g^- = T_g^+ = T_g, \tag{1}$$

as are the applied gate voltages

$$V_{gs}^- = V_{gs}^+ = V_g. \tag{2}$$

The governing equations are to be solved in the silicon region

$$|x_1| < T_{si}/2, \qquad 0 < y_1 < L, \tag{3}$$

which becomes

$$|x| < 1, \qquad 0 < y < 1, \tag{4}$$

after introducing the scaling

$$x_1 = \frac{T_{si}}{2}\, x, \qquad y_1 = Ly. \tag{5}$$

In the silicon, charge densities due only to the electrons will be considered, as the acceptor doping is considered weak. There are two physical variables: ψ, the electrostatic potential, and ϕ_n, the quasi-Fermi potential for electrons. In these circumstances, Gauss' equation is

$$\epsilon_{si}\left(\frac{\partial^2\psi}{\partial x_1^2} + \frac{\partial^2\psi}{\partial y_1^2}\right) = q\, n_i\, e^{(\psi-\phi_n)/V_{th}}, \tag{6}$$

where ϵ_{si} is the dielectric constant of silicon, q is the electron charge, n_i is the intrinsic carrier concentration, and V_{th} is the thermal voltage.

The conservation of current due to electrons reads

$$\frac{\partial}{\partial x_1}\left(e^{(\psi-\phi_n)/V_{th}}\,\frac{\partial\phi_n}{\partial x_1}\right) + \frac{\partial}{\partial y_1}\left(e^{(\psi-\phi_n)/V_{th}}\,\frac{\partial\phi_n}{\partial x_2}\right) = 0. \tag{7}$$

It is now propitious to introduce a scaling for the potentials ψ, ϕ_n. We put

$$(\psi, \phi_n) = V_{max}(w, \phi), \tag{8}$$

where we assume that there is a maximum applied voltage V_{max}. Subsequently we take $V_{max} = 2$ volts. With the scaling adopted in (5) and (8) the field equations (6), (7) may be written

$$2\left(\frac{\partial^2 w}{\partial x^2} + \gamma^2\frac{\partial^2 w}{\partial y^2}\right) = e^{(w-\phi-\alpha)/\epsilon}, \tag{9}$$

$$\frac{\partial}{\partial x}\left(e^{(w-\phi)/\epsilon}\frac{\partial\phi}{\partial x}\right) + \gamma^2\frac{\partial}{\partial y}\left(e^{(w-\phi)/\epsilon}\frac{\partial\phi}{\partial y}\right) = 0, \tag{10}$$

where

$$\gamma = \frac{T_{si}}{2L}, \qquad \epsilon = \frac{V_{th}}{V_{max}}, \qquad e^{-\alpha/\epsilon} = \frac{qn_i T_{si}^2}{2\epsilon_{si} V_{max}}. \tag{11}$$

The two devices shown in Figure 2 have $T_{si} = 10$ nm, $L = 10$ nm, and 20 nm, giving $\gamma = 1/2$, $1/4$, respectively. With $V_{th} = 0.0259$ V and V_{max} taken to be 2 V, the value of ϵ is $0.013 \approx 1/77$. For $T_{si} = 10$ nm, the value of α is 0.277.

2.1. Boundary conditions.

2.1.1. Source/Drain BCs. The values of the quasi-Fermi potential at these boundaries are the applied voltages. The source voltage is taken to be zero, and the drain voltage V_{ds}, giving

$$\phi_n = 0 = \phi \qquad \text{at } y = 0, \tag{12}$$

$$\phi_n = V_{ds}, \quad \phi = \phi_d = V_{ds}/V_{max} \qquad \text{at } y = 1. \tag{13}$$

The source and drain are both p-n junctions with electrostatic potential differences there due to the discontinuity in doping density levels. This is called the built-in voltage, ψ_{bi}. The boundary conditions on the electrostatic potential at these interfaces are then

$$\psi = \psi_{bi} \quad \text{or} \quad w = \psi_{bi}/V_{max} = w_{bi} \qquad \text{at} \quad y = 0, \tag{14}$$

$$\psi = \psi_{bi} + V_{DS} \quad \text{or} \quad w = w_{bi} + \phi_d \qquad \text{at } y = 1. \tag{15}$$

2.1.2. Gate BCs. The devices under consideration are taken to be symmetric about $x = 0$, so the boundary conditions at $x_1 = -T_{si}/2$ may be inferred from those applied at $x_1 = T_{si}/2$. The gate oxide is an insulator allowing no current to cross it, so

$$\frac{\partial \phi_n}{\partial x_1} = 0 = \frac{\partial \phi}{\partial x} \qquad \text{at } x = 1. \tag{16}$$

The gate voltage, V_{GS}, is applied at the boundary $x_1 = T_g + T_{si}/2$. Continuity of electrostatic potential and displacement at $x_1 = T_{si}/2$, and the linear potential profile in the insulator, yield

$$\epsilon_{si} \frac{\partial \psi}{\partial x_1} = \epsilon_{ox}(V_{GS} - \psi)/T_g \qquad \text{at } x_1 = T_{si}/2, \tag{17}$$

or in scaled variables (with $v_g = V_g/V_{max}$)

$$\frac{\partial w}{\partial x} = r(v_g - w) \qquad \text{at } x = 1, \text{ where } r = \frac{\epsilon_{ox} T_{si}}{2\epsilon_{si} T_g}. \tag{18}$$

Since only the solution in the central part of the device away from the gate oxide regions is addressed in this presentation, the boundary conditions at the gates at $x = \pm 1$ are not invoked.

3. Central section ODEs. Figure 2 indicates that there is a large region of the device where the profile of electron density from gate to gate is quite flat. There are steep deviations from this behavior in narrow regions adjacent to the gates. Here, a positive gate voltage has attracted a high density of electrons to "channel" regions,

the terminology used in the single-gated case. These regions will be addressed subsequently as boundary layers in the manner introduced in [4, 16]. In this section we develop a solution for the central section where we assume that the potentials w and ϕ are functions only of y. By putting

$$2\gamma^2 = e^{-\beta/\epsilon} \quad \text{and} \quad \chi = w - \phi + \beta - \alpha, \tag{19}$$

where $\beta - \alpha = \epsilon \ln[\epsilon(L/L_D)^2/2]$ with L_D is the Debye length, 24 microns for silicon, (9)–(10) may then be written as

$$\frac{\partial^2 \chi}{\partial y^2} + \frac{\partial^2 \phi}{\partial y^2} = e^{\chi/\epsilon}, \tag{20}$$

$$\frac{\partial}{\partial y}\left(e^{\chi/\epsilon}\frac{\partial \phi}{\partial y}\right) = 0. \tag{21}$$

Equation (21) integrates to

$$\frac{\partial \phi}{\partial y} = Ae^{-\chi/\epsilon}, \tag{22}$$

where A is a constant. It represents the (scaled) current density; its dependence on the dimensions of the double gate and the voltage difference between source and drain ($y = 0$ and $y = 1$) is the target of this work. A first-order system is achieved by setting

$$s = \frac{\partial \chi}{\partial y}, \qquad t = \frac{\partial \phi}{\partial y} \tag{23}$$

and it follows that

$$\frac{\partial t}{\partial y} = -\frac{st}{\epsilon}, \qquad \frac{\partial s}{\partial y} = \frac{A}{t} + \frac{st}{\epsilon}. \tag{24}$$

Dividing these gives

$$\frac{ds}{dt} = -1 - \frac{A\epsilon}{st^2} \quad \text{or} \quad s\frac{ds}{dt} + s = -\frac{\epsilon A}{t^2}. \tag{25}$$

An alternative formulation is obtained by eliminating s from (24) yielding

$$\epsilon\frac{d^2t}{dy^2} = \frac{\epsilon}{t}\left(\frac{dt}{dy}\right)^2 + t\frac{dt}{dy} - A. \tag{26}$$

Also useful was the equation for the inverse function $y(t)$ which supplied us with some preliminary results.

Equation (25) is an Abel ODE of the second kind, and there are exact (parametric) solutions to it in terms of Bessel functions of order 1/3; see [12]. Maple supplies solutions in terms of Airy functions. These are given in section 6.

There are two-point boundary conditions on the primary variables, but these conditions do not provide direct boundary information for (25). For the analysis presented here it is assumed that the solution trajectory passes through $s = 0$, $t = t_c > 0$ and that the trajectory spans $-\infty < s < \infty$, $0 < t \le t_c$.

A solution trajectory for $s(t)$, relevant for the boundary-value problem, is shown in Figure 3. Graphs of ϕ, χ, s, t as functions of y are shown in Figure 4.

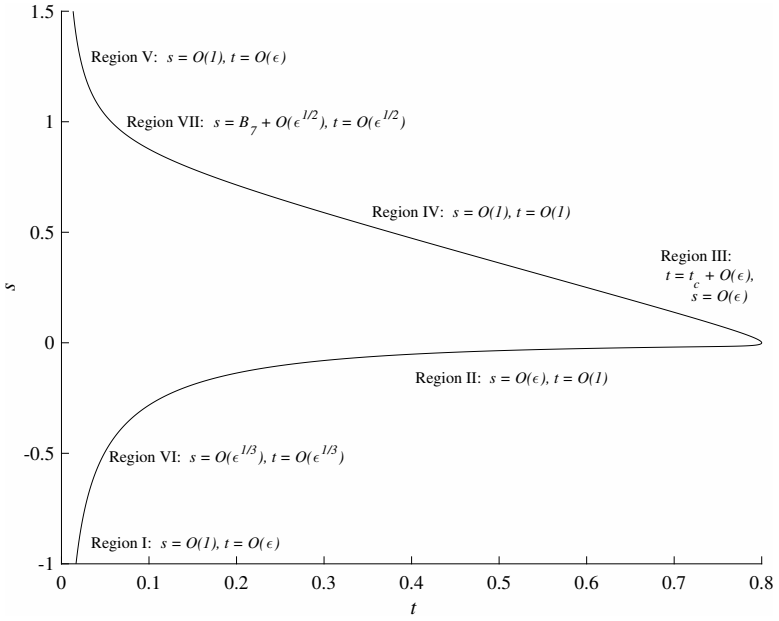

FIG. 3. *Typical $s(t)$ from* (25) *for double gate application.*

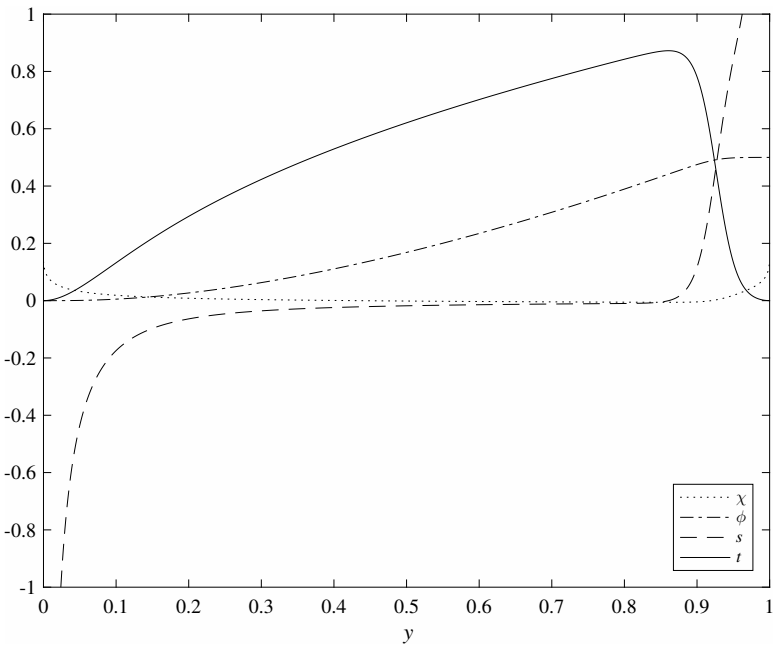

FIG. 4. *Typical solutions for* (23)–(24) *with* $\epsilon = 1/77$, $\chi_s = 0.138$, *and* $\phi_d = 0.5$.

The next two sections contain solutions to the ODEs (23)–(25). The first, an approximate solution for the ODE (25), is developed from the MAE approach based on $\epsilon \ll 1$. This solution is extended to ϕ and χ in section 5 using (23). It has the advantage that it provides explicit formulae for the dependent functions ϕ and χ in

terms of y, and the boundary conditions (12)–(13) also enter explicitly. The ODEs constitute a fourth-order system with two boundary conditions at $y = 0$ and two at $y = 1$. Equation (22) constitutes one first integral, with A representing the electron flux density crossing $y =$ constant. The full solution will relate A to the applied drain voltage, ϕ_d, in the BCs, and hence the current/voltage characteristic across the central section of the device.

The second solution, section 6, is predicted first from the Airy function solution to the first-order ODE (25). Subsequently, and remarkably, we present two further integrals. These three integrals, together with (22), provide an *exact solution* to the fourth-order system (20)–(21). These solutions are complicated and not explicit. However for $\epsilon \ll 1$, with information on variable behavior provided by the MAE solution, and otherwise, we are able to provide current characteristics to a higher-order approximation than does the first-order MAE one derived.

4. Matched asymptotic expansion (MAE) solution for $s(t)$. We now proceed to obtain solutions to (25) in limited regions that are identified by various scalings for the variables. A more comprehensive solution is then sought by matching and joining these solutions using standard MAE techniques [5, 10, 13]. Although this approach runs into difficulties (due to matching) that requires a less formal solution, the MAE approach brings valuable insight both in overall structure and in local behavior.

Only the first terms in the expansions are given. Five regions are obvious from Figure 3:

- Region I has $s < 0$, $s = O(1)$, $t = O(\epsilon)$, $y = O(\epsilon)$, $\phi = O(\epsilon^2)$, $y = O(\epsilon)$.
- Region II has $s < 0$, $s = O(\epsilon)$, $t = O(1)$, $\phi = O(1)$, $y = O(1)$.
- Region III has $s = O(\epsilon)$, $t = t_c + O(\epsilon)$, $\phi = \phi_c + O(\epsilon^2)$, $y = y_c + O(\epsilon)$.
- Region IV has s, t both $O(1)$ in $s > 0$, $\phi = \phi_d + O(\epsilon)$, $y = O(1 - \epsilon)$.
- Region V has $s > 0$, $s = O(1)$, $t = O(\epsilon)$, $\phi = \phi_d + O(\epsilon^2)$, $y = O(1 - \epsilon)$.

The subscript c refers to quantities at $t = t_c$, the maximum of t. We see from Figure 4 that $\phi_c = \phi_d + O(\epsilon)$. Subsequently, two more regions are identified: Region VI between I and II, and Region VII between IV and V, the latter being barely used. In fact, the boundary condition on χ, which leads to one on t from (22), shows that t is exponentially small near the boundaries. However, the scaling close to the boundary remains the same as in Regions I and V, and there is no need to consider a different scaling.

4.1. Asymptotic expansions for Regions I–V for $s(t)$. Straightforward expansions in power series in ϵ are given below.

Region I. With $s = O(1)$ and $t = O(\epsilon)$ the first-order solution is

$$s = -\left[\frac{2\epsilon A}{t} - J_1^2\right]^{1/2}, \tag{27}$$

where J_1 is a constant, taken to be real, based on the numerical solution.

Region II. With $s = O(\epsilon)$ and $t = O(1)$

$$s = -\frac{\epsilon A}{t^2}. \tag{28}$$

Region III. With $s = O(\epsilon)$ and $t = t_c + O(\epsilon)$,

$$t = t_c - s + \frac{\epsilon A}{t_c^2} \ln\left(\frac{t_c^2 s}{\epsilon A} + 1\right), \tag{29}$$

where the constant of integration has been chosen so that $t = t_c$ at $s = 0$. The inverse of this solution is

$$s = -\frac{\epsilon A}{t_c^2}\left[1 + W\left(-\exp\left\{-1 + \frac{t_c^2}{\epsilon A}(t - t_c)\right\}\right)\right], \tag{30}$$

where W is the Lambert function [3].

Region IV. With s, t both $O(1)$

$$s = B_4 - t. \tag{31}$$

Region VII. With $s = B_7 + O(\epsilon^{1/2})$, $t = O(\epsilon^{1/2})$

$$s = B_7 - t + \frac{A\epsilon}{B_7 t} + \epsilon^{1/2} C_7. \tag{32}$$

Region V. This is similar to Region I, leading to

$$s = \left[\frac{2\epsilon A}{t} + J_5^2\right]^{1/2}. \tag{33}$$

4.2. Matching for Regions I–V and VII. Using the standard technique for matching [5] we obtain the following results. Matching solutions in III, IV, and V yields

$$B_4 = t_c \quad \text{and} \quad J_5 = B_4, \tag{34}$$

respectively. The first result requires the use of the W_{-1} branch of the Lambert function, for which $W_{-1}(x) \sim \ln(-x)$ for $x \ll 1$. Matching VII with IV and V shows that $B_7 = B_4$. The quantity C_7 cannot be determined at this order of approximation, but Region VII is not used in what follows. Composite solutions in $s > 0$ may now be generated.

For IV–V.

$$s = -t + \left[B_4^2 + \frac{2\epsilon A}{t}\right]^{1/2}. \tag{35}$$

For III–IV.

$$s = -\frac{\epsilon A}{B_4^2}\left[1 + W_{-1}\left(-\exp\left\{-1 + \frac{B_4^2}{\epsilon A}(t - B_4)\right\}\right)\right]. \tag{36}$$

For III–V.

$$s = \left[B_4^2 + \frac{2\epsilon A}{t}\right]^{1/2} - B_4 + \frac{\epsilon A}{B_4^2}\left[-1 - W_{-1}\left(-\exp\left\{-1 + \frac{B_4^2}{\epsilon A}(t - B_4)\right\}\right)\right]. \tag{37}$$

For II–III. Matching solutions for II, III is successful. Here the W_0 branch of the Lambert function is used, with $W_0(x) \sim x$ for $x \ll 1$.

For I–II. Matching solutions for I, II is not possible. A bridging solution is necessary. It is clear from the $t \gg \epsilon$ behavior of (27) that $J_1 \ll 1$ and that the Region I and II solutions meet in a region where s and t are $O(\epsilon^{1/3})$. Hence we introduce Region VI, between Regions I and II with the change of variable

$$S = (\epsilon A)^{-1/3} s, \qquad T = (\epsilon A)^{-1/3} t. \tag{38}$$

Under this scaling (3.7) becomes

$$S \frac{dS}{dT} + S = -1/T^2. \tag{39}$$

That is, the same equation is reproduced.

In order to proceed with the MAE solution to (25) in $s < 0$, it is necessary to match a solution of (39) with the solutions in Regions I and II, i.e., (27) and (28). This requires asymptotic properties of solutions to (39). The exact solutions (Bessel functions) are complicated and their properties with respect to input parameters are not easily accessible. Thus a direct approach to solving (25) by MAE is obstructed in $s < 0$ and we pursue an alternative, approximate solution.

4.3. Alternative to MAE solution in $s < 0$. We have information on the behavior of $s(t)$ in $s < 0$, namely, (27), (28). Moreover, direct numerical solutions to (25), and the exact solutions implemented numerically, both imply that $J_1 \ll 1$. Taking $J_1 = 0$, $s = -[2\epsilon A/t]^{1/2}$ for $t \ll 1$ and $s = -\epsilon A/t^2$for $s \ll 1$. A smooth function having these properties is

$$s = -\left[\left(\frac{t}{2\epsilon A}\right)^{1/2} + \frac{t^2}{\epsilon A}\right]^{-1}. \tag{40}$$

Comparison of (40) with numerical solutions to (25) shows excellent agreement for a wide range of t, except in the neighborhood of $s = 0$, $t = t_c$. It would be useful to improve its accuracy in the neighborhood of $s = 0$, $t = t_c$, thereby anchoring the approximation. The local solution there is available, (29) or (30). After some numerical experimentation, we chose to include in (40) a local approximation that passes through $s = 0$, $t = t_c$, but is small elsewhere. This is

$$s = -\left[\left(\frac{t}{2\epsilon A}\right)^{1/2} + \frac{t^2}{\epsilon A} + \frac{2\epsilon A}{t_c^2(t_c - t)}\right]^{-1}. \tag{41}$$

Figure 5 shows the approximation (41) for $s < 0$ and the MAE composite formula (37) for $s > 0$ for the values $t_c = 0.4$ and $t_c = 0.9$ with $\epsilon A = 0.01$. We do not use (40) or (41) directly in the matching of § 5, in particular because (41) leads to an unacceptable singularity in ϕ, but given their accuracy for $s(t)$, we work with a similar hybrid solution for $t(y)$.

5. An approximate MAE solution for ϕ and χ. The inability to match the solutions to (25) for $s(t)$ across Regions I and II, exposed in section 3.2, provides a precursor to similar problems when solutions for the primary variables ϕ and χ as functions of y are sought. These solutions may be found from (23), (24) together with

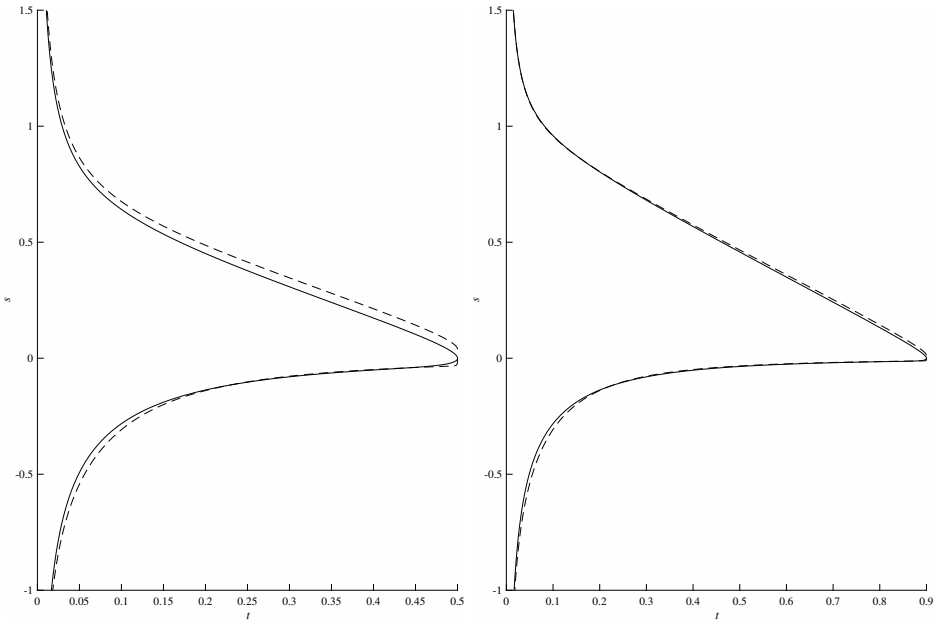

FIG. 5. *Numerical solution (solid) and MAE solution (dashed) for* $s(t)$ *with* $t_c = 0.5$ *(left) and* $t_c = 0.9$ *(right) for* $\epsilon A = 0.01$.

the solutions for $s(t)$ obtained in the various region in the section above. It was found necessary, as a result, to make approximations to the ideal MAE approach, akin to (40). Our approach to matching is semiformal, in that we keep terms of orders 1 and, e.g., $\epsilon^{1/3}$ and $\epsilon^{2/3}$ together, with terms of $O(\epsilon \log \epsilon)$ and higher being viewed as the next term in expansions.

A typical numerical solution for the variables ϕ, χ, s, t as functions of y is shown in Figure 4. The changes in ϕ are small in Regions I and V, that is, in regions where $y = O(\epsilon)$ and $y = 1 - O(\epsilon)$ near the source and drain, respectively. However, changes in χ and s in these regions are substantial and are required to be modeled accurately. Also, finding ϕ, χ in Region III from (29) or (30) is difficult. As Region III is small, an approximation based on intersecting Regions II and IV is made. These properties are achieved in the following results. Integration constant subscript numbers identify the region (except subscript c is used in Region III, indicating "corner").

Region I.

$$s = -J_1 \cot\{J_1[y/\epsilon + K_1]/2\}, \tag{42}$$

$$t = \frac{2A\epsilon}{J_1^2} \sin^2\{J_1[y/\epsilon + K_1]/2\}, \tag{43}$$

$$\phi = N_1 - \frac{A\epsilon^2}{J_1^3} \sin\{J_1[y/\epsilon + K_1]\} + \frac{A\epsilon y}{J_1^2}, \tag{44}$$

$$\chi = -\epsilon \ln\{(2\epsilon/J_1^2) \sin^2\{J_1[y/\epsilon + K_1]/2\}. \tag{45}$$

This solution has a singularity when $y = O(\epsilon^{2/3})$, that is in Region VI. It should be matched to the solution there, but we have no good asymptotic information on the latter.

We know that $J_1 = O(\epsilon^{1/3})$. Hence we can obtain a leading-order solution that is of the same order of validity by neglecting J_1. This is useful for later. The result is

$$s = -\frac{2\epsilon}{y + \epsilon K_1}, \tag{46}$$

$$t = \frac{A}{2\epsilon}(y + \epsilon K_1)^2, \tag{47}$$

$$\phi = \frac{A}{6\epsilon}[(y + \epsilon K_1)^3 - (\epsilon K_1)^3], \tag{48}$$

$$\chi = -\epsilon \ln \frac{(y + \epsilon K_1)^2}{2\epsilon}. \tag{49}$$

Region VI. No simplification is possible in the $s(t)$ relation, so we cannot obtain a simple solution. This is the reason for the hybrid approach presented below.

Region II.

$$s = -\frac{\epsilon}{2(y - y_2)}, \tag{50}$$

$$t = \sqrt{2A(y - y_2)}, \tag{51}$$

$$\phi = (8A/9)^{1/2}(y - y_2)^{3/2} + Q_2, \tag{52}$$

$$\chi = -\frac{\epsilon}{2} \ln \frac{2(y - y_2)}{A}, \tag{53}$$

where y_2 and Q_2 are constants of integration.

Region I–II *hybrid.*

$$t_H = \left[(2Ay)^{-1/2} + \frac{b}{y^{3/2}} + \frac{2\epsilon d}{Ay^2}\right]^{-1} + A \exp(-\chi_s/\epsilon), \tag{54}$$

$$\phi = \int_0^y t_H(y')\, dy'. \tag{55}$$

These formulae satisfy the boundary conditions at $y = 0$. We will not need χ and s. The form (54) satisfies the boundary condition at $y = 0$, but also matches with (47) near the origin when $d = 1$ because of the y^2 term if the exponential term is neglected. The dominant contribution to ϕ comes from Region II, so we can use b to improve the accuracy in that region by matching (51) and (54). In the same vein, we can also pick d to match to the correction term to (51), which can be shown to be $(y - y_2)^{-1}$. The result will no longer be such a good match near the origin in Region I, but this is acceptable since $\phi = O(\epsilon^2)$ there. Using the fact that $y_2 = O(\epsilon^{2/3})$, the appropriate relation is

$$\sqrt{2Ay}\left(1 - \frac{y_2}{2y} + O(y_2^2)\right) + \frac{\epsilon}{y}[1 + O(y_2)] = \sqrt{2Ay}\left(1 - \frac{b\sqrt{2A}}{y} - \frac{2\epsilon d\sqrt{2A}}{Ay^{3/2}} + O(\epsilon^2)\right). \tag{56}$$

The $O(y_2)$ terms match if we take $b = y_2/2\sqrt{2A}$. Pursuing the matching to the next order order leads to $d = -1/4$, but a negative value for d leads to unwanted singularities in the approximant (54). It is not immediately clear what value to take for d: the improvement in ϕ is $O(\epsilon)$ over Region II, but the contribution to ϕ from Region VI is also $O(\epsilon)$. Based on numerical experiments, we set $d = 0$, which leads to simplifications in (55). It turns out to be more important for the hybrid solution to be accurate in Region III than in Region I.

Region III. Here $s(t)$ reverses direction at $s = 0$ and $t(y)$ achieves a maximum; see Figures 3 and 4. We denote by (y_c, ϕ_c, χ_c) the values of these variables at this corner. Local expansions at this point, together with (3), give

$$s = \frac{\epsilon A}{B_4^2}[\exp[B_4(y - y_c)/\epsilon] - 1], \tag{57}$$

$$t = B_4 + \frac{A}{B_4}(y - y_c) - \frac{\epsilon A}{B_4^2}[\exp[B_4(y - y_c)/\epsilon] - 1], \tag{58}$$

$$\phi = \phi_c + \left[B_4 + \frac{\epsilon A}{B_4}\right](y - y_c) + \frac{A}{2B_4}(y - y_c)^2 - \frac{\epsilon^2 A}{B_4^3}[\exp(B_4(y - y_c)/\epsilon) - 1], \tag{59}$$

$$\chi = \chi_c - \frac{\epsilon A}{B_4^2}(y - y_c) + \frac{\epsilon^2 A}{B_4^3}[\exp(B_4(y - y_c)/\epsilon) - 1]. \tag{60}$$

Note that $\chi_c = -\epsilon \log(B_4/A)$. For matching purposes the following inverse is useful:

$$y = y_c + \frac{B_4}{A}(t - B_4) - \frac{\epsilon}{B_4} - \frac{\epsilon}{B_4} W\left(-\exp\left[\frac{B_4^2}{A\epsilon}(t - B_4) - 1\right]\right). \tag{61}$$

Region IV.

$$s = B_4[1 + (A/B_4C_4)\exp(B_4(1 - y)/\epsilon)]^{-1}, \tag{62}$$

$$t = B_4[1 + (B_4C_4/A)\exp(-B_4(1 - y)/\epsilon)]^{-1}, \tag{63}$$

$$\phi = N_4 - \epsilon \ln[1 + (A/B_4C_4)\exp(B_4(1 - y)/\epsilon)], \tag{64}$$

$$\chi = \epsilon \ln[A/B_4 + C_4 \exp(-B_4(1 - y)/\epsilon)]. \tag{65}$$

Region V.

$$s = J_5 \coth\{J_5[(1 - y)/\epsilon + K_5]/2\}, \tag{66}$$

$$t = \frac{2A\epsilon}{J_5^2}\sinh^2\{J_5[(1 - y)/\epsilon + K_5]/2\}, \tag{67}$$

$$\phi = N_5 - \frac{A\epsilon^2}{J_5^3}\sinh\{J_5[(1 - y)/\epsilon + K_5]\} + A\epsilon(1 - y)/J_5^2, \tag{68}$$

$$\chi = -\epsilon \ln\left\{\frac{2\epsilon}{J_5^2}\sinh^2\{J_5[(1 - y)/\epsilon + K_5]/2\right\}. \tag{69}$$

The solutions presented above for Regions I–V using the hybrid solution (54)–(55) involve the unknown constants A, y_c, ϕ_c, χ_c, B_4, C_4, N_4, J_5, K_5, N_5, and y_2. By omitting Region V for the changes in ϕ (the solution for ϕ in Region IV is used to satisfy the boundary condition at $y = 1$), there is no need to evaluate N_5. Also χ_c is not related to the other constants. There are 9 constants remaining. Matching solutions in adjacent regions and boundary conditions are used to obtain further relations between the constants.

Boundary conditions.

$$\text{At } y = 1, \text{ on } t \text{ or } \chi: \quad (2\epsilon/J_5^2)\sinh^2(J_5K_5/2) = \exp(-\chi_s/\epsilon), \tag{70}$$

$$\text{At } y = 1, \text{ on } \phi: \quad \phi_d = N_4 - \epsilon \ln[1 + A/B_4C_4]. \tag{71}$$

The boundary conditions at the origin have already been incorporated into (54)–(55).

Matching. Regions I–II and III: This uses the hybrid solution in I–II and matches it to the solution in III.

$$t\text{:}\quad y_c = \frac{B_4^2}{2A} + y_2, \tag{72}$$

$$\phi\text{:}\quad \phi_c = \phi(y_c) = 2\sqrt{2A}\left[\frac{2}{3}y_c^{3/2} - \frac{y_2}{2}y_c^{1/2} + \left(\frac{y_2}{2}\right)^{3/2}\tan^{-1}\left(\frac{2y_c}{y_2}\right)^{1/2}\right]. \tag{73}$$

The matching in t uses t from II, since (51) from II and the hybrid form (54) agree to $O(\epsilon)$ from (56). The matching in ϕ uses the hybrid solution (55) at $y = y_2$. We have dropped the exponential term in (54) since it is small (see below).

Regions III and IV:

$$y\text{:}\quad y_c = 1 - \frac{\epsilon}{B_4}\ln\frac{C_4 B_4^4}{A^2\epsilon}. \tag{74}$$

This result can be obtained using the W_{-1} branch of the Lambert function.

Regions IV and V:

$$s \text{ and } \chi\text{:}\quad B_4 = J_5 = \frac{1}{K_5}\ln\frac{2J_5^2}{C_4\epsilon}. \tag{75}$$

An eighth equation is obtained from applying the formula for $\phi(y)$ in Region IV at $y = y_c$, assuming little variation in ϕ in Region III. This gives

$$\phi_c = N_4 - \epsilon\ln\{1 + (A/B_4C_4)\exp B_4(1 - y_c)/\epsilon\}. \tag{76}$$

Equations (70)–(76) provide 8 equations for the determination of the 9 constants to be evaluated in terms of the input ϕ_d.

Further approximation. Assuming that $B_4 = J_5$ is $O(1)$ and approximating the hyperbolic sine function for small argument in (70) then gives $K_5 \sim \sqrt{2/\epsilon}e^{-\chi_s/2\epsilon}$, and thus K_5 may be neglected. With the built-in voltage V_{bi} given by $V_{th}\ln(N_D/n_i)$ for the source and drain doped at a level $N_D = 10^{23}$/c.c. and the silicon at intrinsic level 10^{10}/c.c., the term $e^{-\chi_s/\epsilon}$ is $O(10^{-5})$. Then (75) gives that $C_4 = 2B_4^2/\epsilon$. This is the same approximation used to obtain the hybrid solution in I–II and matching (72)–(73).

Finding y_2. The value of y_2 remains to be found. It is known to be of order $\epsilon^{2/3}$, so the first approximation is to set it zero. From the forms of Region VI and of (51), we can write $Ay_2 = \lambda(\epsilon A)^{2/3}$, where λ should be a constant independent of A. The question then becomes the value of λ. Numerical solutions of the full problem show that $\lambda \approx 3$. (We shall find the exact value of λ from asymptotics of the exact integrals in section 6 below, and the result $\lambda \approx 3$ is verified.)

Solution for A and B_4. With $C_4 = 2B_4^2/\epsilon$, (74) provides y_c in terms of A and B_4. This can be combined with (72) to give

$$y_c = 1 - \frac{\epsilon}{B_4}\ln\frac{2B_4^6}{A^2\epsilon^2} = \frac{B_4^2}{2A} + \lambda\epsilon^{2/3}A^{-1/3}, \qquad y_2 = \lambda\epsilon^{2/3}A^{-1/3}. \tag{77}$$

The second equality provides a relation between A and B_4. A second relation between A and B_4 comes from the difference of (71) and (76), using the relation (73) for ϕ_c. The result is

$$\phi_d = \epsilon\ln\frac{1 + B_4^3/A\epsilon}{1 + A\epsilon/2B_4^3} + 2\sqrt{2A}\left[\frac{1}{3}y_c^{3/2} - \frac{y_2}{2}y_c^{1/2} + \left(\frac{y_2}{2}\right)^{3/2}\tan^{-1}\sqrt{2y_c/y_2}\right]. \tag{78}$$

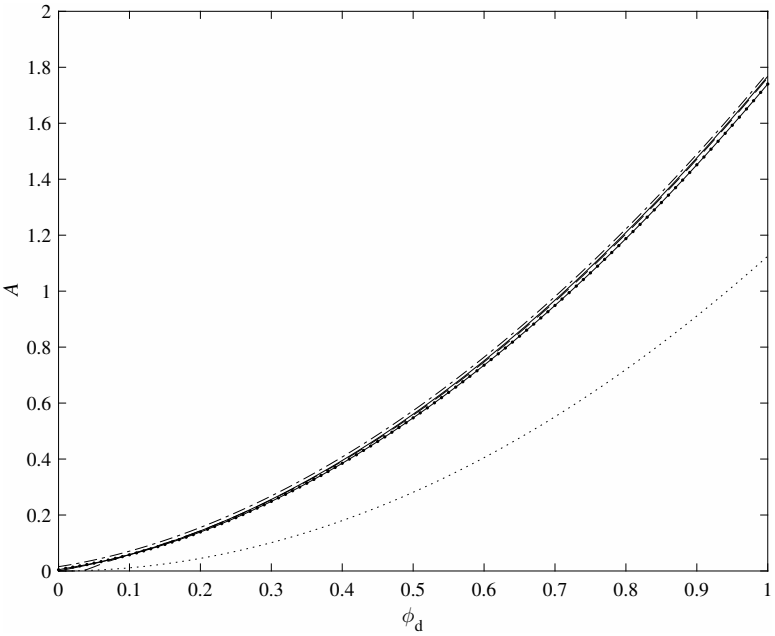

FIG. 6. *Current density A as a function of ϕ_d: numerical solution (solid curve), solution of* (77)–(78) *(dashed curve); leading-order approximation $A = (9/8)\phi_d^2$ (dotted curve); approximation* (79) *(dash-dot curve); and approximation* (99) *(solid curve with overlaid dots) for $\epsilon = 1/77$.*

Equations (77) and (78) are to be solved, given ϵ and ϕ_d for A and B_4. Then A is a measure of the current flowing from source to drain in response to the applied drain voltage, given by ϕ_d. Numerical solutions of (77)–(78) for A as a function of ϕ_d with $\epsilon = 1/77$ and $\epsilon = 1/33$ are shown in Figures 6 and 7, along with the relation between A and ϕ_d obtained from the numerical solution to the original ODEs (23), (25). Also shown is the approximation obtained by ignoring higher-order terms in (77)–(78), yielding $y_c = 1$, $B_4^2 = 2A$, and $\phi_d = 2\sqrt{2A}/3$, i.e., $A = (9/8)\phi_d^2$. A more accurate approximation can be obtained from (78) by neglecting terms of $O(\epsilon \ln \epsilon)$ and higher, leading to

$$\phi_d = \left(\frac{8A}{9}\right)^{1/2} \left[1 - \frac{3}{2} y_2\right]. \tag{79}$$

Figure 8 compares the value of A corresponding to $\phi_d = 0.5$ as ϵ decreases.

6. Complete integrals in the central section. We now derive the exact solution for $s(t)$ obtained by Maple using a simple change of variable, and go further by obtaining an explicit solution to the full problem. We start from the two coupled nonlinear first-order ODEs of (24), and define the new variable $u = s + t$. Then

$$\frac{du}{dy} = \frac{A}{t}, \tag{80}$$

where we now use a total rather than a partial derivative since we are not concerned with variations in the x-direction. A further differentiation gives

$$\epsilon \frac{d^2u}{dy^2} = u \frac{du}{dy} - A, \tag{81}$$

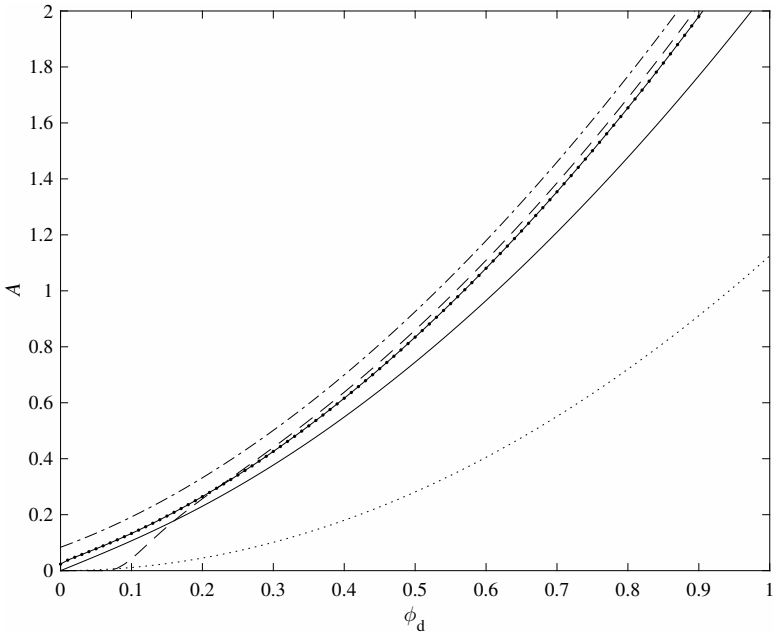

FIG. 7. *Current density A as a function of ϕ_d: numerical solution (solid curve), solution of* (77)–(78) *(dashed curve); leading-order approximation $A = (9/8)\phi_d^2$ (dotted curve); approximation* (79) *(dash-dot curve); and approximation* (99) *(solid curve with overlaid dots) for $\epsilon = 1/33$.*

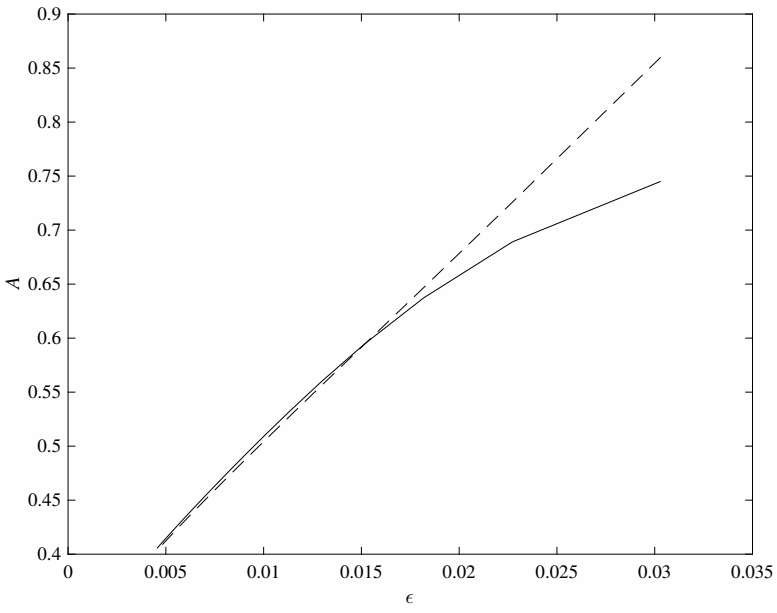

FIG. 8. *Current density A for $\phi_d = 0.5$ as a function of ϵ: numerical solution (solid curve), solution of* (77)–(78) *(dashed curve).*

which integrates to

$$\epsilon\frac{du}{dy} = \frac{1}{2}u^2 - A(y - y_*), \tag{82}$$

where y_* is a constant of integration satisfying

$$(t_0 + s_0)^2 - \frac{2\delta}{t_0} = -2Ay_* \tag{83}$$

on evaluating (82) at $y = 0$ and using (81), defining $\delta = A\epsilon$.

Equation [9] shows that the nonlinear equation

$$\frac{dW}{dz} + W^2 = z \tag{84}$$

has the solution $W = w^{-1}dw/dz$, where $d^2w/dz^2 = zw$. Hence we write $u = \alpha W(z)$ and $z = \beta(y - y_*)$ and identify (82) with (84). Solving for α, β, and z gives

$$\alpha = -(4\delta)^{1/3}, \qquad \beta = \left(\frac{A}{2\epsilon^2}\right)^{1/3}, \qquad z = \frac{1}{4}\left(\frac{2}{\delta}\right)^{2/3} 2A(y - y_*). \tag{85}$$

The solution for $w(z)$ may be written without loss of generality as $w = \mathrm{Ai}(z) - C\,\mathrm{Bi}(z)$, where C is a constant and $\mathrm{Ai}(z)$ and $\mathrm{Bi}(z)$ are the Airy functions of the first and second kind, respectively. Hence

$$u = s + t = -(4\delta)^{1/3}\frac{\mathrm{Ai}'(z) - C\,\mathrm{Bi}'(z)}{\mathrm{Ai}(z) - C\,\mathrm{Bi}(z)}. \tag{86}$$

This can be written as an implicit relation in the form

$$\frac{2^{1/3}(t + s)\,\mathrm{Ai}(z) + 2\delta^{1/3}\,\mathrm{Ai}'(z)}{2^{1/3}(t + s)\,\mathrm{Bi}(z) + 2\delta^{1/3}\,\mathrm{Bi}'(z)} = C. \tag{87}$$

We also note that (82) can be written as

$$z = \frac{1}{4}\left(\frac{2}{\delta}\right)^{2/3} 2A(y - y_*) = \frac{1}{4}\left(\frac{2}{\delta}\right)^{2/3}\left[(s + t)^2 - \frac{2\delta}{t}\right], \tag{88}$$

and this is the expression for z in (87) used by Maple. Note that Maple was solving the system (25) for $s(t)$, rather than the full system for $s(y)$ and $t(y)$. The fact that z is an affine function of y is the key to further progress.

We can now integrate (86). The result is

$$[\mathrm{Ai}(z) - C\,\mathrm{Bi}(z)]e^{A(\phi+\chi)/2\delta} = E, \tag{89}$$

where E is a constant of integration. We now evaluate C at $y = 0$, giving

$$C = \frac{2^{1/3}(t_0 + s_0)\,\mathrm{Ai}_0 + 2\delta^{1/3}\,\mathrm{Ai}_0'}{2^{1/3}(t_0 + s_0)\,\mathrm{Bi}_0 + 2\delta^{1/3}\,\mathrm{Bi}_0'}, \tag{90}$$

where the 0 subscripts indicate values at $y = 0$. We then substitute this into (89) and

simplify, using the result $\mathrm{Ai}'(z)\,\mathrm{Bi}(z) - \mathrm{Ai}(z)\,\mathrm{Bi}'(z) = \pi^{-1}$, to obtain

$$E = \frac{2\delta^{1/3}\pi^{-1}}{(s_0+t_0)\,\mathrm{Bi}_0 + 2\delta^{1/3}\,\mathrm{Bi}_0'} e^{(\phi_0+\chi_0)/2\epsilon}. \tag{91}$$

We can do the same at $y = 1$, replacing the subscript 0 by 1. Noting that $\chi_0 = \chi_1$, $\phi_0 = 0$ and $\phi_1 = \phi_d$, and dividing the two results gives

$$e^{\phi_d/2\epsilon} = \frac{(s_1+t_1)\,\mathrm{Bi}_1 + 2\delta^{1/3}\,\mathrm{Bi}_1'}{(s_0+t_0)\,\mathrm{Bi}_0 + 2\delta^{1/3}\,\mathrm{Bi}_0'}. \tag{92}$$

The result (89) is a new integral of the equations of motion. Crucially it gives access to the boundary conditions that concern ϕ and χ. It can be used to obtain A as a function of ϕ_d, one of the main goals of this work, without having to solve a boundary-value problem. This approach allows one to reach smaller values of ϵ, which cause trouble for the numerical solution because of the presence of boundary layers. It is convenient to take A as known and obtain ϕ_d in terms of A. The procedure is as follows. Evaluating (87) at $y = 0$ and $y = 1$ gives a single equation that can be solved for y_* given A. This uses the result (83) to express s at the boundaries in terms of $yz - 0$ and $t = Ae^{-\chi/\epsilon}$ there; the choice of sign that comes from the square root in $s = -t \pm (2\delta/t - 2Ay_*)^{1/2}$ is uniquely determined since $s < 0$ ($-$ sign) at $y = 0$ and $s > 0$ ($+$ sign). Given y_*, (92) can be solved to give ϕ_d in terms of A.

We can obtain an asymptotic result for small ϵ. Near $y = 1$, z_1 is asymptotically large, so we can replace the Airy functions by their (exponentially large) asymptotic values. However, near $y = 0$, it turns out that z_0 is $O(1)$. Taking the logarithm of (92), we obtain

$$\frac{\phi_d}{2\epsilon} = \frac{2}{3}z_1^{3/2} + \log\left[\frac{z_1^{-1/4}}{\sqrt{\pi}} \frac{(s_1+t_1)(1+O(z_1^{-3/2})) + 2\delta^{1/3}z_1^{1/2}(1+O(z_1^{-3/2})}{(s_0+t_0)\,\mathrm{Bi}_0 + 2\delta^{1/3}\,\mathrm{Bi}_0'}\right]. \tag{93}$$

The leading-order approximation to this equation gives

$$\phi_d \sim \frac{4}{3}\epsilon z_1^{3/2} = \left(\frac{8A}{9}\right)^{1/2}(1-y_*)^{3/2}. \tag{94}$$

This can be compared to (79). We now need to find y_*.

To do this we examine C near $y = 0$ and $y = 1$. Near $y = 1$, the derivative terms in the numerator and denominator in (87) are small, so

$$C \sim \frac{\mathrm{Ai}_1}{\mathrm{Bi}_1} \sim \frac{1}{2}e^{-4z_1^{3/2}/3}. \tag{95}$$

This is exponentially small, so near $y = 0$ the numerator of C must be small, i.e., $2^{1/3}(s_0+t_0)\,\mathrm{Ai}_0 \sim -2\delta^{1/3}\,\mathrm{Ai}_0'$. The first term dominates, so $z_0 \sim a_1 \approx -2.338\ldots$, the first zero of the Airy function. This shows that $y_* = O(\delta^{2/3})$, and more precisely

$$y_* \sim -(2\delta^2)^{1/3}\frac{a_1}{A}. \tag{96}$$

In Region II, comparing the asymptotic result $t \approx \sqrt{2A(y-y_2)}$ from (51) and $t^2 \approx 2A(y-y_*)$ from (85) shows that y_2 and y_* are the same. Hence $\lambda = -2^{1/3}a_1 = 2.9458\ldots$, justifying the approximate value of 3 that was employed earlier.

We can find the correction to y_* (actually to z_0) by writing $z_0 = a_1 + \zeta$. Then $\mathrm{Ai}(z_0) = \zeta\,\mathrm{Ai}'(a_1) + O(\zeta^2)$. We also use $s_0 + t_0 = -(2\delta/t_0)^{1/2} + e.s.t$, since t_0 is exponentially small. Then (87) and (95), including errors terms, become

$$C = \frac{1}{2}e^{-4z_1^{3/2}/3}[1 + O(z_1^{-3/2})] = \frac{2^{1/2}(s_0+t_0)\zeta\,\mathrm{Ai}'(a_1) + 2\delta^{1/3}\,\mathrm{Ai}'_(\,a_1) + \cdots}{2^{1/3}(s_0+t_0)\,\mathrm{Bi}(a_1) + 2\delta^{1/3}\,\mathrm{Bi}'(a_1) + \cdots}. \tag{97}$$

This shows that the correction term arises from the numerator of the fraction vanishing again, giving

$$\zeta \sim (2/\delta)^{1/6} t_0^{1/2} = (2/\delta)^{1/6} A^{1/2} e^{-\chi_S/2\epsilon}, \tag{98}$$

an exponentially small correction. This shows that higher corrections to ϕ_d come from expanding the logarithm in (93) to higher algebraic order.

Finally we note that (94) and (96) can be combined to give

$$A \sim \frac{9}{8}\left[\phi_d^{2/3} - \left(\frac{16}{9}\right)^{1/3} a_1 \epsilon^{2/3}\right]^3. \tag{99}$$

7. Conclusion(s). As far as the authors are aware there have been no analytic solutions published for the drift-diffusion equations (20), (21). The results achieved here provide both an exact solution, and an approximate one based on the MAE approach for small ϵ. The exact integrals are complicated. The simpler MAE results provide accurate formulas, in particular for the source-to-drain current flow, and they indicate how to approach the exact results for information. Part II will include the effects of a gate voltage as a boundary layer in order for a model to be completed for general operating use of the device. These results will be useful in further applications related to the double-gate geometry, for example, to tunnel field-effect transistors.

Acknowledgments. The authors acknowledge helpful conversations with Marina Chugunova, Glenn Ierley, Saleh Tanveer, Shigeyasu Uno, and Lindsay Skinner.

REFERENCES

[1] H. Abebe, E. Cumbertach, H. Morris, V. Tyree, T. Numata, and S. Uno, *Symmetric and asymmetric double gate MOSFET modeling*, J. Semicond. Tech. Sci., 9 (2009), pp. 225–232.
[2] Q. Chen, E. M. Harrell, and J. D. Meindl, *A physical short-channel threshold voltage model for undoped symmetric double-gate MOSFETs*, IEEE Trans. Electron Devices, 50 (2003), pp. 1631–1637.
[3] R. M. Corless, G. H. Gonnet, D. E. G. Hare, D. J. Jeffrey, and D. E. Knuth, *On the Lambert W function*, Adv. Comput. Math., 5 (1996), pp. 329–359.
[4] E. Cumberbatch, H. Abebe, and H. Morris, *Current-voltage characteristics from an asymptotic analysis of the MOSFET equations*, J. Engrg. Math., 39 (2001), pp. 25–46.
[5] J. Kevorkian and J. D. Cole, *Multiple Scale and Singular Perturbation Methods*, Springer, New York, 1996.
[6] S. Kolberg and T. A. Fjeldy, *2D modelling of nanoscale double gate silicon-on-insulator MOSFETs using conformal mapping*, Phys. Scr., T126 (2006), pp. 57–60.
[7] X. Liang and Y. Taur, *A 2-D analytical solution for SCEs in DG MOSFETs*, IEEE Trans. Electron Devices, 51 (2004), pp. 1385–1391.
[8] H. Lu and Y. Taur, *An analytic potential model for symmetric and asymmetric DG MOSFETs*, IEEE Trans. Electon Devices, 53 (2006), pp. 1161–1168.
[9] F. W. J. Olver, D. W. Lozier, R. F. Boisvert, and C. W. Clark, eds., *NIST Handbook of Mathematical Functions*, Cambridge University Press, New York, 2010.
[10] R. E. O'Malley, *Singular Perturbation Methods for Ordinary Differential Equations*, Springer, New York, 1991.

[11] A. Ortiz-Conde, F. J. Garciz-Sanchez, J. Muci, S. Malobabi, and J. J. Liou, *A review of core compact models for undoped double-gate SOI MOSFETs*, IEEE Trans. Electron Devices, 54 (2006), pp. 131–140.
[12] A. D. Polyanin and V. F. Zaitsev, *Handbook of Exact Solutions for Ordinary Differential Equations*, 2nd ed., Chapman & Hall/CRC Press, New York, 2003.
[13] L. A. Skinner, *Singular Perturbation Theory*, Springer, New York, 2011.
[14] S. Uno, *personal communication*, 2009.
[15] M. J. Ward, *Singular perturbations and a free boundary problem in the modeling of field-effect transistors*, SIAM J. Appl. Math., 52 (1992), pp. 112–139.
[16] M. J. Ward, F. M. Odeh, and D. S. Cohen, *Asymptotic methods for metal oxide semiconductor field effect transistor modeling*, SIAM J. Appl. Math., 50 (1990), pp. 1099–1125.